A Novel Dynamic Hysteresis Model for Grain-Oriented Electrical Steels Based on Magnetic Domain Theory

Zhi Zhang, Hamed Hamzehbahmani, and Philip H. Gaskell

Department of Engineering, Durham University, Durham DH1 3LE, U.K.

A novel approach is adopted to model the hysteresis phenomenon of grain-oriented electrical steels (GOESs), by incorporating a variation of the domain patterns associated with ferromagnetic materials during magnetization and demagnetization. The ensuing model treats the anisotropic and isotropic components separately, together with the coupling effect of the excitation field. Its ability to replicate experimentally obtained dynamic hysteresis loops (DHLs) for Epstein size laminations of GO 3% SiFe electrical steels, for different magnetizing frequencies and peak flux densities, and facilitate the straightforward evaluation of the energy loss in GOESs is demonstrated for the case of controlled sinusoidal magnetic induction. Close agreement is found to exist between the predicted energy loss and corresponding bulk measurements, with the maximum difference being less than 2%.

Index Terms— **Dynamic modeling, energy loss, ferromagnetic materials, grain-oriented electrical steels (GOES), magnetic hysteresis.**

I. Introduction

GRAIN-ORIENTED electrical steels (GOESs) are silicon steels in which strong magnetic properties exist in the rolling direction of production in the material's plane. Consequently, GOES laminations are widely used in industry for producing distribution and power transformers, reactors, and large turbo generators, where energy efficiency and high performance are essential [1]. As to the future, improved electrical machines and new infrastructure will prove essential in addressing the urgency surrounding the need for increased renewable energy integration into existing power systems, in which GOESs will continue to play a vital role. Accordingly, data analysis of magnetization measurements and accurate modeling of the magnetic properties of GOESs are critical to investigate the performance of the materials involved in the practice.

The magnetization of such materials can be analyzed by means of the hysteresis phenomenon. In this respect, the well-known 1-D diffusion equation, linking the magnetic field strength H and the magnetic flux density B through the material resistivity ρ, has been used for decades for the dynamic modeling of electrical steels [2]

$$\frac{\partial B}{\partial t} = \rho \frac{\partial^2 H}{\partial x^2}. \tag{1}$$

However, this equation was developed when the concept of magnetic domains had yet to be proposed [3]. It describes a homogeneous medium and, hence, is rarely used alone as a hysteresis model for magnetic materials. In practice, electrical steels are inhomogeneous, containing grains and magnetic domains [4], [5]; accordingly, the total energy loss calculated using (1) will invariably be lower than the corresponding measured value [2].

Manuscript received July 24, 2021; revised October 19, 2021; accepted November 13, 2021. Date of publication November 16, 2021; date of current version December 22, 2021. Corresponding author: Z. Zhang (e-mail: zhi.zhang@durham.ac.uk).

Color versions of one or more figures in this article are available at https://doi.org/10.1109/TMAG.2021.3128765.

Digital Object Identifier 10.1109/TMAG.2021.3128765

A widely adopted approach to characterize magnetic materials is the utilization of a static hysteresis model (SHM) coupled to an eddy current one to accurately predict the magnetic loss and magnetization behavior. An alternative approach for evaluating the magnetization process of electrical steels is based on the statistical energy loss separation principle proposed by Bertotti [6]. In this approach, the total energy loss of the material, P_t, is expressed as

$$P_t = P_{\text{hys}} + P_{\text{eddy}} + P_{\text{exc}} \tag{2}$$

where P_{hys} is the static hysteresis component, P_{eddy} is the classical eddy-current loss, and P_{exc} is the excess loss [2]. The latter, P_{exc}, is argued to be a result of the competition between the external magnetic field and the opposite field induced by eddy currents and microstructural interactions [6]. The physical basis of the energy loss separation principle is founded on the dynamic behavior of ferromagnetic cores in operation, which is due to a combination of hysteresis, classical eddy currents, domain wall motion, skin effect, and saturation [7].

The model proposed by Jiles and Atherton (J-A) [8], [9] assumes that hysteresis is caused by overcoming the impedance pinning of domain wall motion. It can be used as an SHM instead of the measured static hysteresis loop (SHL). Their model consists of two differential equations representing irreversible and reversible differential susceptibilities, whose combination results in the total differential susceptibility. In the J-A model, the basic an-hysteretic magnetization equation is derived for homogeneous isotropic materials. However, this idealistic magnetic material is not suitable for inhomogeneous anisotropic structures. Ramesh *et al.* [10] and Szewczyk [11] extended the J-A model for the case of anisotropic magnetic materials by introducing anisotropic energy to the an-hysteretic magnetization equation, making it possible to trace their magnetic hysteresis.

Other mathematical models, such as the scalar Preisach model and the vector Preiscah model [12], or the stop and play models [13], are not linked to the physics of magnetic

materials: their implementation is cumbersome due to a large number of measurements or hysterons needed to superpose the operators with a weighting or shape function [14]. Despite this, the Preisach model represents magnetic hysteresis with reasonable accuracy for the tracing of hysteresis loops, which has led to its subsequent wide use for the analysis of magnetization.

Zirka *et al.*'s [15] model uses experimentally established magnetization rules, i.e., flux density congruency of the reversal curves; the latter, to any arbitrary order, is constructed using the major hysteresis loop. Prior to this, Zirka *et al.* [16] proposed a model using the congruency property, present in the derivation of the Preisach model, to construct a history-dependent hysteresis model (HDHM). Their model is based on the internal segments of the first-order reversal curves. A history-independent hysteresis model (HIHM) is characterized in which any order reversal curves are determined by the current reversal point and generated directly leading to the major curves of the loop [17].

This article presents a new analytical model in the form of a single equation to describe the magnetic behavior and dynamic performance of GOESs. Its distinguishing feature is in embodying the microstructure of the magnetic material, i.e., the domain patterns, enabling the modeling of dynamic hysteresis loops (DHLs) with a high degree of accuracy. Another advantage is its simple implementation in tracking the DHL. It can also be used to characterize magnetizing processes and perform an energy loss analysis for GOESs.

II. Problem Formulation

Derivation of the theoretical underpinning of the new model differs from previous work: it is based on the postulation that the hysteresis field occurs at any order reversal point when the directions of the magnetic field strength H and the magnetic flux density B are changed. On the assumption that the excitation field $h(t)$ is the vector summation of the hysteresis field H_h generated from the magnetization coupling effect at the turning point and the magnetic field $H(t)$ triggered from the excitation source, it leads to

$$h(t) = H(t) + H_{h.} \tag{3}$$

The direction of H_h is aligned with that of the previous magnetization at the turning point and is opposite to the reversed magnetic field. H_h is used to remove the hysteresis effect from H during magnetization to obtain $h(t)$, and H_h is equal to the coercivity or coercive force H_c but acting in the opposite direction, $H_h = -H_c$. In that case, (3) becomes

$$h(t) = H(t) - H_c. \tag{4}$$

Accordingly, unlike the conventional methods used to describe the hysteresis phenomenon in terms of $B - H$ loops, the approach adopted here utilizes in preference $B - h$ curves, which can conveniently be formed from experimentally measured $H(t)$ and H_c values.

GOESs consist of both anisotropic and isotropic domain patterns, which, in a demagnetized state, forms closed structures so that no external magnetic field is revealed. When magnetized, the magnetic properties are dominated by the anisotropic components during magnetization because the grains are mainly aligned in the rolling direction, which forms a strong anisotropic structure leading to an easy magnetizing direction.

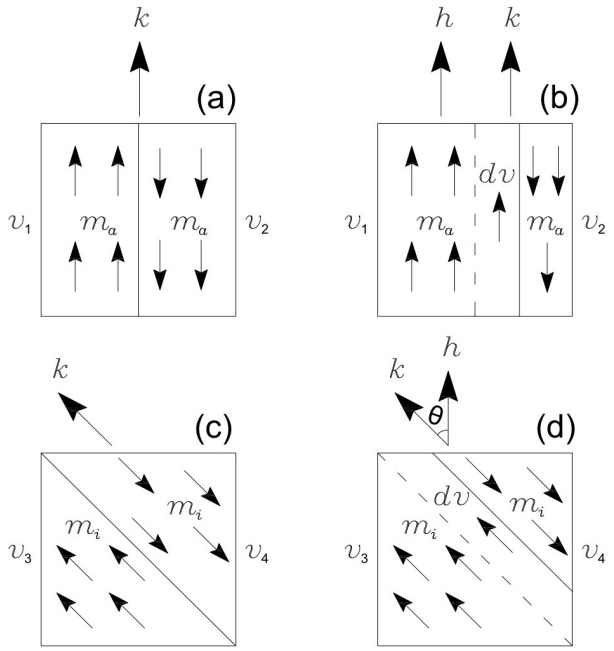

Fig. 1. Typical domain patterns for ferromagnetic materials. Top row anisotropic case: (a) demagnetized state and (b) in the presence of an excitation field. Bottom row isotropic case: (c) demagnetized state and (d) in the presence of an excitation field.

Fig. 1 shows a schematic of the demagnetized [(a) and (c)] and magnetized [(b) and (d)] domain states for ferromagnetic materials, representing anisotropic and isotropic domains, respectively. In order to describe the magnetizing processes in the presence of an excitation field $h(t)$ for both domain patterns, it is assumed that a unit domain with a magnetic moment per unit volume, which, in Fig. 1(a), is expressed as m_a and, in Fig. 1(c), as m_i, represents a typical domain.

The magnetic moment of the anisotropic domain in Fig. 1(a) is aligned with the rolling direction, coincidentally with the same direction as the anisotropic direction k_a, where υ_1 and υ_2 are the number of the unit domain moment m_a. For the corresponding isotropic domain, as shown in Fig. 1(c), υ_3 and υ_4 are the numbers of the unit domain moments m_i. In a demagnetized state, υ_1 and υ_2 are equal. However, when $h(t)$ is applied, the magnetic moment $M_1 = m_a\upsilon_1$ in the domain is aligned with the excitation field increases, while the domain moment $M_2 = m_a\upsilon_2$ opposite to $h(t)$ reduces due to the domain wall motion, as illustrated in Fig. 1(b). The alignment of the domain in Fig. 1(c) varies randomly from domain to domain, whereas the domain's direction could be aligned with the easy crystallographic axis direction, which depends on whether the crystallographic axis is preferred by the magnetic moments. In Fig. 1(d), the excitation field $h(t)$ does not align with the anisotropic direction k_a, and there is an arbitrary angle θ between them.

During magnetization for the domain pattern of Fig. 1(a), the domain wall only moves, along with the direction, to enlarge the volume of the domain aligned with the field

due to the strong uniaxial anisotropy. There is no domain rotation in Fig. 1(b) because both domain directions and anisotropic directions are aligned with the excitation field direction. By comparison, the domain in Fig. 1(d) encounters rotation before nucleation or after unification; in that case, the isotropic domain suffers more energy losses in order to rotate the domain direction pointing at the excitation field direction.

Allowing for the Zeeman effect [18], the energies due to the magnetic moment per unit volume for anisotropic and isotropic domains under an excitation field h are

$$E_a = -\mu_0 m_a \cdot h \tag{5}$$

and

$$E_i = -\mu_0 m_i \cdot h \tag{6}$$

respectively, where μ_0 is the permeability of the free space between the magnetic domains. The new model is based on expressing the energy changes in these two domain patterns in the presence of an excitation field. The total magnetic moments in a typical anisotropic and isotropic domain with unit domain number υ can be expressed as

$$M_a = m_a \upsilon \tag{7}$$

and

$$M_i = m_i \upsilon \tag{8}$$

respectively.

According to statistical thermodynamics, in a state of thermal equilibrium at temperature T, the probability of a domain having energy E is proportional to the Boltzmann factor $\exp(-E/kT)$, where k is Boltzmann's constant. The unit volume number in a domain is then given by the following expression:

$$\upsilon = c \exp\left(-\frac{E}{kT}\right) \tag{9}$$

where c is a constant of proportionality. With reference to Fig. 1(b), the number of the unit moment in the domain aligned with the excitation field can then be expressed as

$$\upsilon_1 = c \exp\left(-\frac{E_1}{kT}\right) \tag{10}$$

while the number of the unit moment in the domain opposite to the excitation field is

$$\upsilon_2 = c \exp\left(-\frac{E_2}{kT}\right). \tag{11}$$

As shown in Fig. 1(b), the number of the unit moment parallel to the excitation field will increase due to the domain wall moving from the dashed line to the solid line position, and the number of the unit moment antiparallel to the field will decrease by the same amount. During the magnetizing process, the increased $d\upsilon$ number of the unit domain along with the excitation field is calculated as

$$d\upsilon = \upsilon_1 - \upsilon_2 \tag{12}$$

and the total number of unit moments in the anisotropic domain pattern is expressed as

$$\upsilon = \upsilon_1 + \upsilon_2. \tag{13}$$

By replacing υ with $d\upsilon$ in (8), the magnetization contributed by the anisotropic domain during the process of magnetization is estimated to be

$$M_a = m_a d\upsilon = m_a \upsilon \frac{\upsilon_1 - \upsilon_2}{\upsilon_1 + \upsilon_2}. \tag{14}$$

The magnetization process in the anisotropic domain under the excitation field can then be expressed as

$$M_a = M_{sa} \tanh(ah) \tag{15}$$

where

$$a = \frac{\mu_0 m_a}{kT} \tag{16}$$

is a balance coefficient for anisotropic components between the unit domain magnetic moment and the disordering effect of thermal agitation. M_a, as defined by (15), is the anisotropic component in the magnetizing processes, which is derived from analysis of the anisotropic domain pattern in ferromagnetic materials. $M_{sa} = m_a \upsilon$ is the saturation magnetization of the anisotropic components when the anisotropic domain magnetic moments opposite to the excitation field are all canceled out to form a unified domain aligned with the excitation field.

Regarding the isotropic domains, the magnetic moments are oriented in an arbitrary direction to the excitation field direction. The domains are formed to achieve self-saturation; they will be aligned randomly to form disordered structures with irregular shapes. Under the excitation field $h(t)$, having an angle θ with magnetic domain moment, the Zeeman energy for the unit domain volume can be expressed as follows:

$$E_i = -\mu_0 m_i h \cos\theta. \tag{17}$$

The number of the corresponding unit domain volume can then be expressed as

$$\begin{aligned} \upsilon &= c \exp\left(\frac{\mu_0 m_i h \cos\theta}{kT}\right) \\ &= c \exp(bh \cos\theta) \end{aligned} \tag{18}$$

where

$$b = \frac{\mu_0 m_i}{kT} \tag{19}$$

is a balance coefficient for isotropic components.

During the magnetizing process in Fig. 1(d), the increased $d\upsilon$ number of the unit domain along with the excitation field is calculated as

$$d\upsilon = \upsilon_3 - \upsilon_4. \tag{20}$$

When $d\upsilon$ approaches 0, the increased $d\upsilon$ number of the unit domain can also be expressed as the derivative of (18); then, the unit volume number differences due to domain wall motion caused by the excitation field in Fig. 1(d) is

$$d\upsilon = -cbh \exp(bh \cos\theta) \sin\theta d\theta \tag{21}$$

leading, on integration, to

$$\upsilon = -cbh \int_0^{\theta} \exp(bh\cos\theta)\sin\theta d\theta. \tag{22}$$

According to (9), the magnetization M_i in the direction of the excitation field in Fig. 1(d) can be obtained from the contribution $m_i \cos\theta$ of the unit domain magnetic moment multiplied by the number of the unit volume domain $d\upsilon$ integrated over the total number, giving

$$M_i = \int_0^{\upsilon} m_i \cos\theta d\upsilon. \tag{23}$$

Combining (22) and (23) leads to

$$\begin{aligned} M_i &= -cbhm_i \int_0^{\Pi} \exp(bh\cos\theta)\sin\theta\cos\theta d\theta \\ &= m_i \upsilon \frac{\int_0^{\Pi} \exp(bh\cos\theta)\sin\theta\cos\theta d\theta}{\int_0^{\Pi} \exp(bh\cos\theta)\sin\theta d\theta}. \end{aligned} \tag{24}$$

Following integration, the magnetization processes of isotropic component M_i, derived from the analysis of the isotropic domain pattern in ferromagnetic materials, in the direction of the excitation field are given by

$$\begin{aligned} M_i &= M_{si}\left(\coth(bh) - \frac{1}{bh}\right) \\ &= M_{si} L(bh) \end{aligned} \tag{25}$$

where $M_{si} = m_i \upsilon$ is the saturation magnetization of the isotropic components when the isotropic domain walls are all eliminated to form a unified domain aligned with the excitation field. The second line of (25) is the well-known Langevin's function [18], which was initially derived according to the microstructures in paramagnetic materials and represents the homogeneous structures in ferromagnetic materials.

The third component in the magnetization processes is the coupling effect of the excitation field, which exists since the initial magnetization but only weakly affects the magnetic induction B. When the ferromagnetic material is subjected to an excitation field, the latter penetrates the material and leads to a coupling effect constituting a proportion of the magnetic induction, which is expressed as

$$M_h = \alpha h \tag{26}$$

where α is the coupling coefficient concerned with the microstructure of the ferromagnetic material; it can be calculated based on relevant measured data. The magnetic induction comprised of the above three components is then acquired as a single generalized equation:

$$B = M_a + M_i + M_h \tag{27}$$

or using (15), (25), and (26) as

$$B = M_{sa}\tanh(ah) + M_{si} L(bh) + \alpha h. \tag{28}$$

The right-hand side of (28) consists of three terms, representing anisotropic, isotropic, and excitation field coupling components, respectively. As pointed out, h is obtained by removing the hysteresis portion from the magnetic field.

The above general physical model is excellent for tracing sigmoid shape curves; however, magnetization processes do not always result in standard smooth regular S-shape curves. When (28) is used to replicate distorted and irregular curves, the differences between modeled and measured curves can prove unacceptable. However, with the recognition that the excitation field coupling effect to the magnetic induction is weak compared to the other two components, in such situations, it can be considered negligible to a good approximation and the hyperbolic tangent together with Langevin's function replaced by an exponential function. This leads to the following simplified expression for the magnetic induction:

$$B = M_{sa}\exp(ah) + M_{si}\exp(bh). \tag{29}$$

Accordingly, (29) can be used to trace the segmented curves in a piecewise manner to achieve piecewise monotonicity when single curves arise with a distorted and irregular shape. Equations (28) and (29) differ from the traditional models used to trace magnetic hysteresis loops directly, in which they are used to track S-shaped single curves obtained from measured hysteresis loops. This new model can interpret the magnetic hysteresis and predict the energy loss of ferromagnetic materials under controlled sinusoidal excitation.

III. Methodology

The proposed model, based on a single equation, (28) or (29), describes the relationship between B and h, in the form of a single curve. Standard methods designed for determining the magnetic properties of electrical steels involve the construction of $B - H$ hysteresis loops via direct measurements, which cannot be used directly in the proposed model. Therefore, as a preliminary step, the excitation field h must be obtained from such experimental data using (4). Determination of the associated parameters, M_{sa} and M_{si}, for use in (28) or (29), based on the microstructures of the magnetic materials, cannot be calculated from the manufacturer's datasheets. Calculating them involves processing the relevant measurement data over the range of measured frequencies and peak flux densities of interest, which was done using MATLAB's curve fitting tool. Once the parameters have been determined, (28) or (29) can then be used to create the required modeled $B - H$ hysteresis loops.

Prior to modeling, experiments were undertaken to measure bulk energy loss and monitor the DHLs of the test samples. Epstein size laminations (30 mm $\times$ 305 mm) of GO 3% SiFe (thickness $d = 0.3$ mm and resistivity $\rho = 0.462$ $\mu\Omega$m) were provided by Cogent Power Ltd., and a standard Single Strip Tester (SST) was used to measure the magnetic properties of the test samples according to BS EN 10280:2001 + A1:2007 [19]. The SST with the test samples represents an unloaded transformer, and the specific energy loss and DHLs for the samples were measured at peak flux densities from 1.0 to 1.7 T, and magnetizing frequencies from 50 to 1000 Hz. In these experiments, the magnetic samples were subjected to an alternating field excitation waveform; a sinusoidal magnetic flux density was achieved by controlling the magnetic field. Uncertainty analysis of the measuring

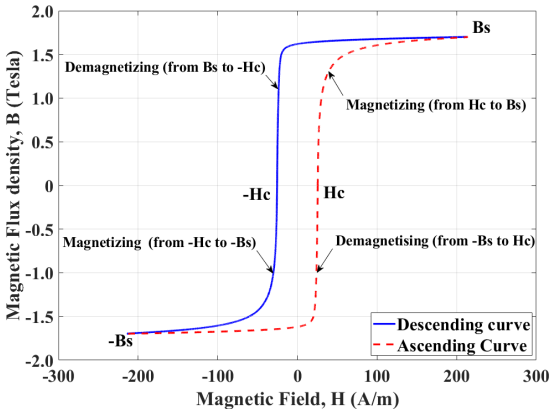

Fig. 2. Measured hysteresis loop for GOES at a frequency of 50 Hz and a peak flux density of 1.7 T.

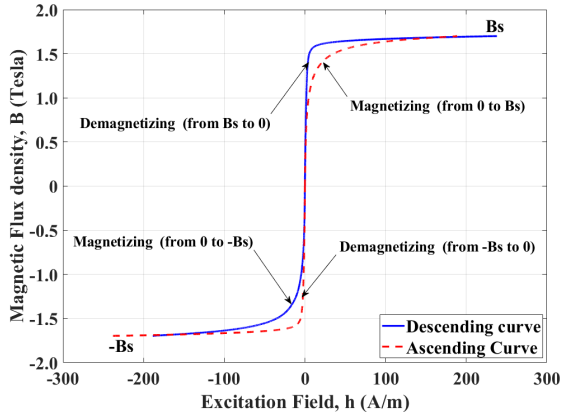

Fig. 3. Single curves for GOES at a frequency of 50 Hz and a peak flux density of 1.7 T, obtained by displacing the measured ascending and descending curve of the hysteresis loop in Fig. 2. an amount H_c to the left and right, respectively.

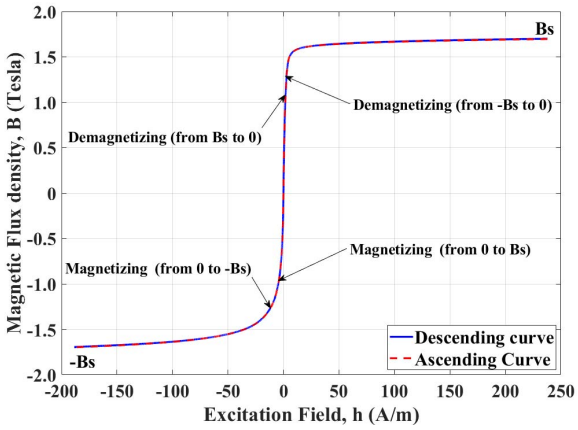

Fig. 4. Overlapping single curves for GOES at a frequency of 50 Hz and a peak flux density of 1.7 T, obtained by rotating the ascending curve through 180° about both the B- and h-axes.

system was performed based on the recommendations given in UKAS M3003 [20]. Type A uncertainty was estimated at ±0.30% and Type B uncertainty at ±0.63%. Further details of the test setup can be found in [21].

IV. Modeling Results

The complexity associated with the modeling of magnetic induction is due, in the main, to the associated hysteresis loop phenomenon, which contributes to a one-to-two relationship from H mapping to B. In the methodology proposed here, this relationship is overcome by treating the curves forming the hysteresis loop as individual descending and ascending sections to achieve a one-to-one injective function, making the tracing of magnetic curves simple. While this procedure avoids having to function the hysteresis loop directly, it is also aligned with exploring the genuine physical meaning of magnetic hysteresis. Hysteresis loops are regarded as lagging behind the phenomenon of magnetization and magnetic induction to the magnetic field. This hysteretic behavior starts at any order reversal point and is caused by the hysteresis field triggered by magnetization coupling effects. The procedure conducted cancels out the hysteresis effect using (4).

As the first step to both illustrate the above procedure and its efficacy, the case of the controlled sinusoidal magnetic induction of a GOES is considered at a magnetizing frequency of 50 Hz and a peak flux density of 1.7 T; subsequent measurements for different frequencies and peak flux densities follow the same methodology. The corresponding measured hysteresis loop shown in Fig. 2 is comprised of two sections: descending and ascending curves. For the descending one, sections B_s to $-H_c$ and $-H_c$ to $-B_s$ represent demagnetization and magnetization curves, respectively; the inverse applies for the ascending curve. Separate curves of B versus h are obtained by displacing the descending curve to the right and the ascending curve to the left a horizontal distance H_c, via (4), as shown in Fig. 3. Note that these now single curves are disconnected at the saturation tips due to the parallel shift of the original descending and ascending sections together with the magnetic field coordinates to the origin.

Both single curves in Fig. 3 pass through the origin (0, 0) establishing a synchronized relationship of B versus h. The modeling of hysteresis loops can now be explored by considering these single curves. The long overlapping section close to the origin represents the similarity between the curves of being dominated by domain wall motion. The dissimilarity between them as they approach the saturation tips reveals the anisotropic characteristics of the steels.

It has long been observed that hysteresis loops are symmetrical about the origin, which makes sense because the magnetic flux density is a sine wave under the controlled magnetic excitation. The next critical step in the processing of the single curves is to rotate the ascending single curve through 180° about both the B- and h-axes, the result of which is shown in Fig. 4. As expected, the descending and ascending curves lay on top of one another following rotation. The key feature of proceeding in this way is that the modeling of hysteresis loops can be achieved by investigating just a single curve, which is a synchronized curve of B versus h given by (28) or (29). The modeled single curve in Fig. 5 is generated using (28) and is indistinguishable from its measured counterpart. The accompanying parameters are calculated separately for the magnetizing and demagnetizing sections of the curve. This is because the domain pattern variations act in the opposite way for the two processes. The associated parameter values are provided in Table I.

TABLE I
PARAMETERS ASSOCIATED WITH (28) FOR OBTAINING THE MAGNETIZING AND DEMAGNETIZING CURVE SECTIONS OF FIG. 5 FOR GOES MAGNETIZED AT A FREQUENCY OF 50 HZ AND A PEAK FLUX DENSITY OF 1.7 T

Curve section	M_{sa} (T)	M_{si} (T)	a	b	α
Magnetizing	0.555	1.007	84.18	23.83	0.072
Demagnetizing	0.790	0.853	56.62	75.74	0.021

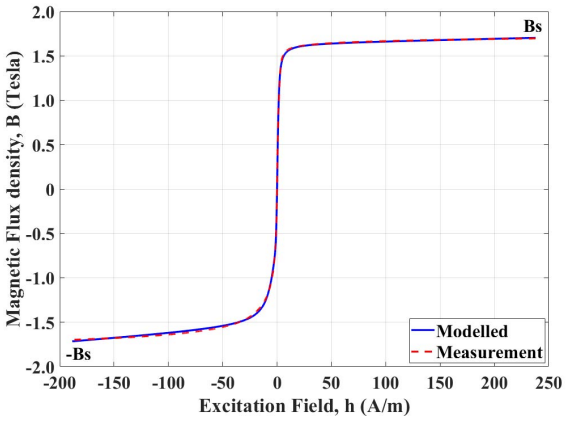

Fig. 5. Superimposed modeled and obtained single curves for GOES at a frequency of 50 Hz and a peak flux density of 1.7 T.

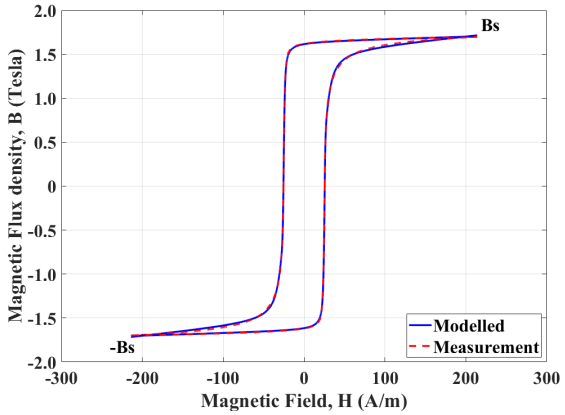

Fig. 6. Measured and modeled hysteresis loop for GOES at a frequency of 50 Hz and a peak flux density of 1.7 T superimposed against the corresponding measured data.

While a key feature of the proposed model is to describe the magnetizing process, the main criterion for verifying the model is to now generate sigmoidal curves representing the corresponding hysteresis loop from the measurement data. Although the model was derived to describe single curves of B versus h, the relevant hysteresis loops of B versus H can be created by reversing the above process, shifting the modeled curves to fit the experimental loops. Comparison between the modeled and measured hysteresis loop is provided in Fig. 6, demonstrating a remarkable degree of agreement.

The most important requirement and test of the new model are its fits to measurement data relating to materials under different magnetizing frequencies and peak flux densities. Accordingly, calculating the modeling parameters involved

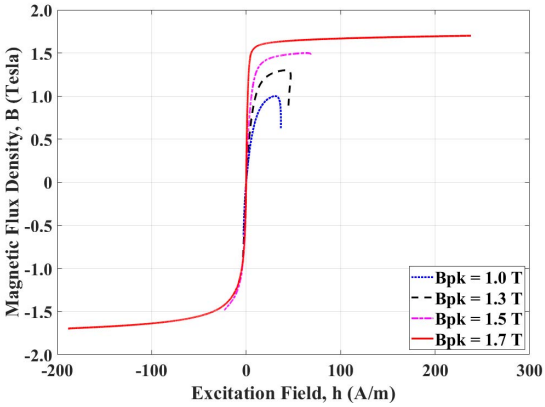

Fig. 7. Single curves obtained, following the same process as in Figs. 2–4, for GOES under sinusoidal excitation at a frequency of 50 Hz and peak flux densities ranging from 1.0 to 1.7 T.

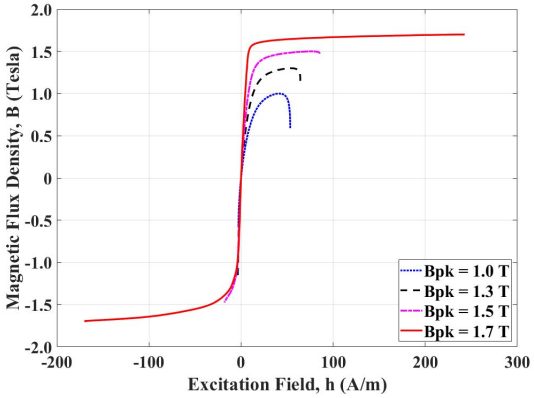

Fig. 8. Single curves obtained for GOES, following the same process as in Figs. 2–4, under sinusoidal excitation at a frequency of 100 Hz and peak flux densities ranging from 1.0 to 1.7 T.

requires the processing of the relevant measurement data for a particular range of magnetizing frequencies and peak flux densities.

The same procedure as explained for a magnetizing frequency of 50 Hz and a peak flux density of 1.7 T is applied for different frequencies and flux densities. First, single curves of B versus h for the test sample were extracted from the measured DHLs. The results for magnetizing frequencies ranging from 50 to 1000 Hz and peak flux densities from 1.0 to 1.7 T are shown in Figs. 7–12, respectively. These curves represent the magnetizing processes for $h < 0$ and demagnetizing processes for $h > 0$. The parameters for these two processes are different, and the calculations need to be performed separately. As shown in Fig. 7, tips of the single curves at a magnetizing frequency of 50 Hz at 1.0 and 1.3 T exhibit deviations due to the asynchronicity.

As the frequency increases, the effect of asynchronicity becomes more evident, which can be seen from the curves displayed in Figs. 8–12 for the different magnetizing frequencies. The resulting distortions of the single curve require the use of (29) to track them in a piecewise manner. The parameters for use in (29) must be determined for each piecewise section; the greater the number of piecewise sections employed, the greater the accuracy of the model. Taking a magnetizing frequency of 800 Hz and a peak flux density of 1.7 T, as a

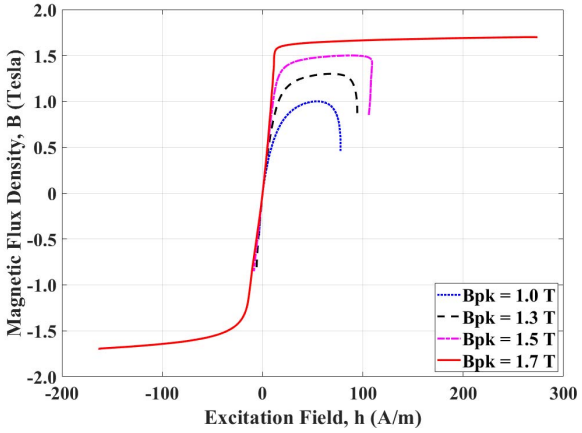

Fig. 9. Single curves obtained for GOES, following the same process as in Figs. 2–4, under sinusoidal excitation at a frequency of 200 Hz and peak flux densities ranging from 1.0 to 1.7 T.

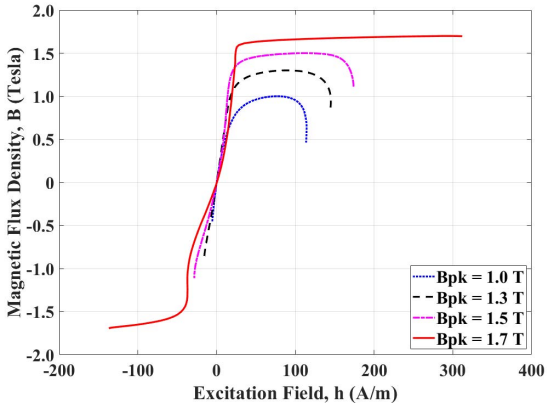

Fig. 10. Single curves obtained for GOES, following the same process as in Figs. 2–4, under sinusoidal excitation at a frequency of 400 Hz and peak flux densities ranging from 1.0 to 1.7 T.

TABLE II

PARAMETERS ASSOCIATED WITH (29) USED TO OBTAIN THE CONTIGUOUS MAGNETIZING AND DEMAGNETIZING CURVE SECTIONS, SIX IN TOTAL, OF FIG. 13 FOR GOES MAGNETIZED AT A FREQUENCY OF 800 HZ AND A PEAK FLUX DENSITY OF 1.7 T

Curve section	M_{sa} (T)	M_{si} (T)	a	b
Magnetizing				
Section 1	-0.143	0.146	-5.757	2.093
Section 2	0	3.656	37.12	-1.279
Section 3	1.449	-4e+5	-0.127	-22.32
Demagnetizing				
Section 4	0.306	-1.866	0.331	0.012
Section 5	4e+13	-1.554	39.14	-0.035
Section 6	0.144	-0.120	5.472	-2.910

typical example, the number of sections required is 6. The associated parameters for this case are provided in Table II.

The magnetizing and demagnetizing curves, and associated modeled sections of each, using (29), are plotted and shown in Fig. 13, while the corresponding parameters for the modeled sections are provided in Table II. Despite the considerable distortion at the tip of the magnetizing curve, the comparison of Fig. 13 confirms the accuracy of the modeling results.

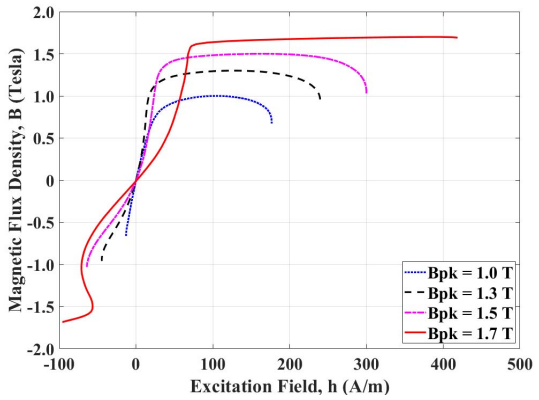

Fig. 11. Single curves obtained for GOES, following the same process as in Figs. 2–4, under sinusoidal excitation at a frequency of 800 Hz and peak flux densities ranging from 1.0 to 1.7 T.

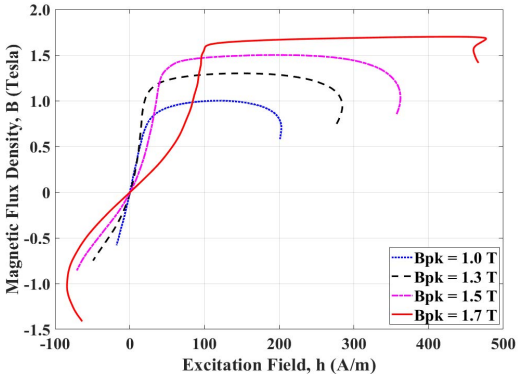

Fig. 12. Single curves obtained for GOES, following the same process as in Figs. 2–4, under sinusoidal excitation at a frequency of 1000 Hz and peak flux densities ranging from 1.0 to 1.7 T.

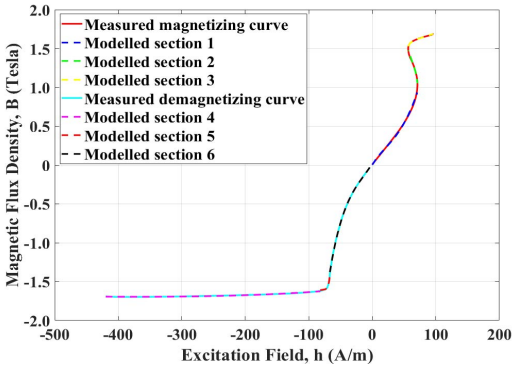

Fig. 13. Modeled contiguous curve sections, 6 in total, superimposed on the corresponding measured single curve for GOES, following the same process as in Figs. 2–5, under sinusoidal excitation at a frequency of 800 Hz and a peak flux density of 1.7 T.

All other such experimentally obtained distorted single curves are processed in the same way.

An interesting feature of the curves shown in Figs. 7–12 is that they have somewhat similar shapes and pass through the origin, which means that the excitation field is partially synchronized with magnetic induction, except for the tips where curl occurs, which dramatically simplifies the investigation of the magnetic properties compared to studying of the $B - H$ loops directly.

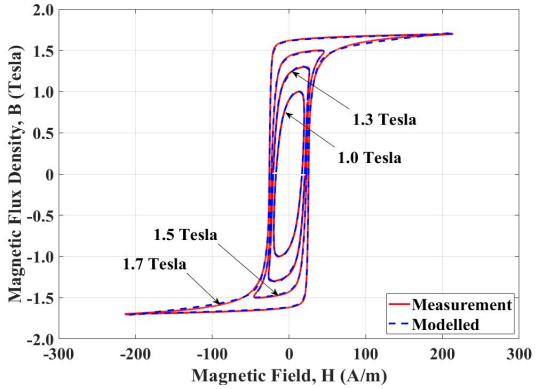

Fig. 14. Modeled hysteresis loops for GOES under sinusoidal excitation at 50 Hz and peak flux densities ranging from 1.0 to 1.7 T superimposed against the corresponding measured data.

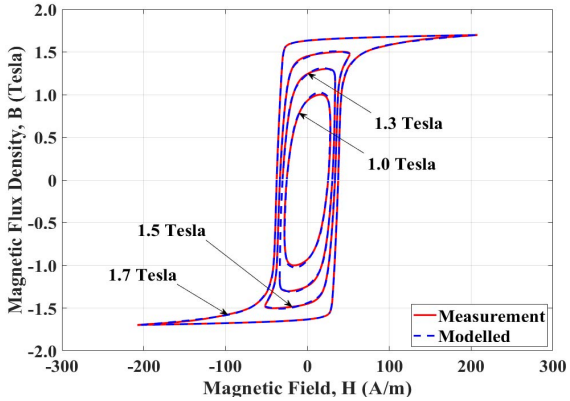

Fig. 15. Modeled hysteresis loops for GOES under sinusoidal excitation at 100 Hz and peak flux densities ranging from 1.0 to 1.7 T superimposed against the corresponding measured data.

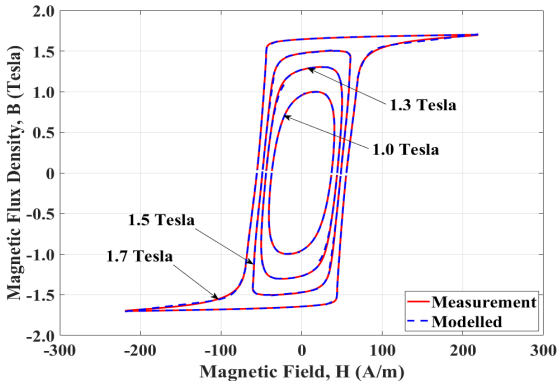

Fig. 16. Modeled hysteresis loops for GOES under sinusoidal excitation at 200 Hz and peak flux densities ranging from 1.0 to 1.7 T superimposed against the corresponding measured data.

The corresponding DHLs for the test sample produced by the model are shown in Figs. 14–19, showing that they coincide exactly with the measured loops for the range of measured frequencies and peak flux densities considered. Equation (28), linking the macroscale features of the magnetic material with the microscale description of domain theories, advances the confirmation of the generalized physical model used in this study.

Conveniently, (28) and (29) can be used to undertake an energy loss evaluation. Unlike the traditional method of

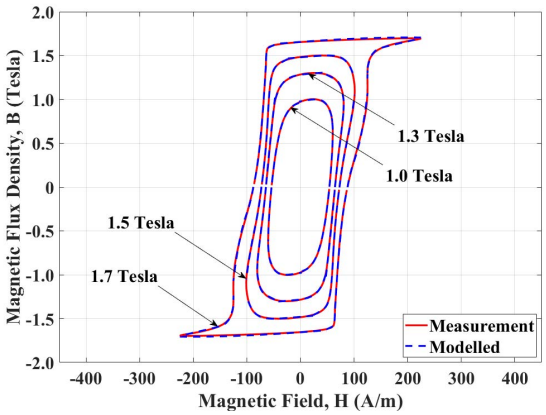

Fig. 17. Modeled hysteresis loops for GO steel under sinusoidal excitation at 400 Hz and peak flux densities ranging from 1.0 to 1.7 T superimposed against the corresponding measured data.

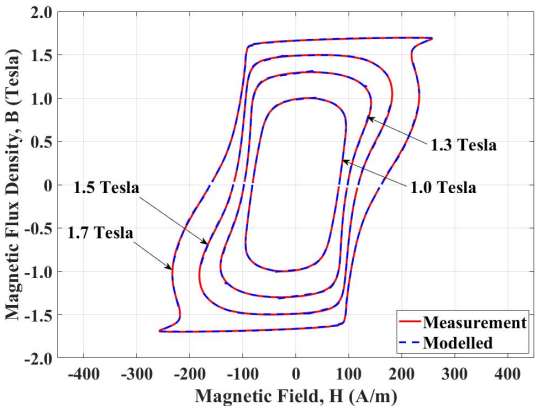

Fig. 18. Modeled hysteresis loops for GOES under sinusoidal excitation at 800 Hz and peak flux densities ranging from 1.0 to 1.7 T superimposed against the corresponding measured data.

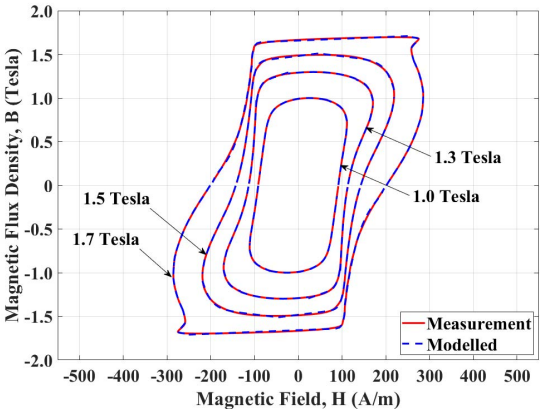

Fig. 19. Modeled hysteresis loops for GOES under sinusoidal excitation at 1000 Hz and peak flux densities ranging from 1.0 to 1.7 T superimposed against the corresponding measured data.

estimating the energy loss by calculating the area within the hysteresis loop, with the present methodology, the total energy loss per cycle can be calculated by simply integrating the model equation, over the range of the excitation field. A comparison between the calculated and measured results, and the percentage difference at the magnetizing frequencies of 50–1000 Hz and the peak flux density of 1.0–1.7 T is provided in Figs. 20 and 21, respectively.

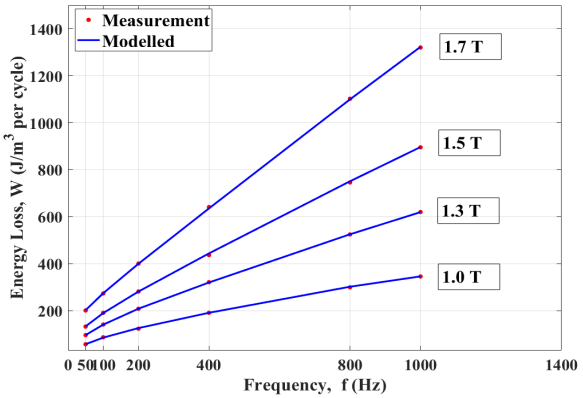

Fig. 20. Comparison between calculated and measured energy losses per cycle for GOESs under sinusoidal excitation at frequencies of 50–1000 Hz and peak flux densities from 1.0 to 1.7 T.

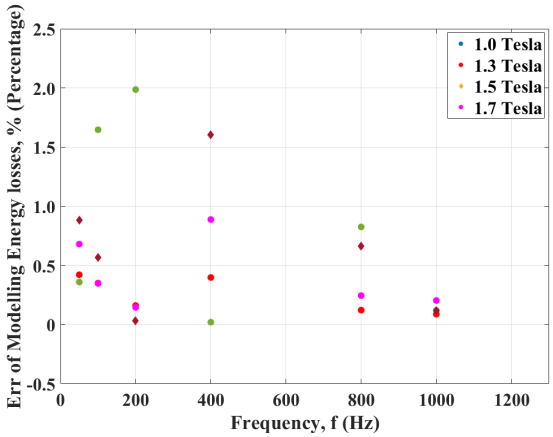

Fig. 21. Energy loss errors for GOESs under sinusoidal excitation at frequencies of 50–1000 Hz and peak flux densities from 1.0 to 1.7 T.

Close agreement with a maximum difference of less than 2% for the range of measurement is observed. It is clear that the new model, based on analyzing single curves, provides an accurate and reliable technique for reproducing the DHLs of GOESs and, hence, for energy loss calculations purposes.

V. Conclusion

A model based on incorporating variation in the domain patterns associated with ferromagnetic materials, treating the anisotropic and isotropic components separately, is derived in the form of a single (28) or (29) when the excitation field coupling effect is omitted. The proposed model is then shown to replicate extremely well experimentally obtained DHLs in the case of Epstein size laminations of GO 3% SiFe electrical steels. This assertion is reinforced via comparisons drawn with corresponding laboratory measurements for a range of magnetizing frequencies and peak flux densities. An additional feature of this single equation is that it enables the total energy loss per cycle to be readily calculated by simply integrating it over the range of the excitation field.

Besides suggesting a significant step forward in the modeling of the magnetization processes associated with soft magnetic materials, it is underpinned by a novel theoretical approach related to DHLs that differs from conventional opinion. The model is equally applicable for the investigation of related magnetic materials, which is underway.

Data Availability

The data that support the findings of this study are available from the corresponding author upon reasonable request.

Acknowledgment

The authors are grateful to Cogent Power Ltd. for providing the electrical steel materials and Cardiff University for the experimental data.

References

[1] P. Beckley, *Electrical Steels: A Handbook for Producers and Users*, 1st ed. Newport, South Wales: European Electrical Steels, 2000.
[2] S. E. Zirka, Y. I. Moroz, A. J. Moses, and C. M. Arturi, "Static and dynamic hysteresis models for studying transformer transients," *IEEE Trans. Power Del.*, vol. 26, no. 4, pp. 2352–2362, Oct. 2011.
[3] J. J. Thomson, "On the heat produced by eddy currents in an iron plate exposed to an alternating magnetic field," *Electrician*, vol. 28, pp. 599–600, 1892.
[4] M. Takezawa, Y. Wada, J. Yamasaki, T. Honda, and C. Kaido, "Effect of grain size on domain structure of thin nonoriented Si-Fe electrical sheets," *IEEE Trans. Magn.*, vol. 39, no. 5, pp. 3208–3210, Sep. 2003.
[5] A. P. S. Baghel, B. S. Ram, K. Chwastek, L. Daniel, and S. V. Kulkarni, "Hysteresis modelling of GO laminations for arbitrary in-plane directions taking into account the dynamics of orthogonal domain walls," *J. Magn. Magn. Mater.*, vol. 418, pp. 14–20, Nov. 2016.
[6] G. Bertotti, "General properties of power losses in soft ferromagnetic materials," *IEEE Trans. Magn.*, vol. MAG-24, no. 1, pp. 621–630, Jan. 1988.
[7] M. Petrun, S. Steentjes, K. Hameyer, and D. Dolinar, "1-D lamination models for calculating the magnetization dynamics in non-oriented soft magnetic steel sheets," *IEEE Trans. Magn.*, vol. 52, no. 3, pp. 1–4, Mar. 2016.
[8] D. C. Jiles and D. L. Atherton, "Theory of ferromagnetic hysteresis," *J. App. Phys.*, vol. 55, no. 6, pp. 2115–2120, 1984.
[9] D. C. Jiles and D. L. Atherton, "Theory of ferromagnetic hysteresis," *J. Magn. Magn. Mater.*, vol. 61, nos. 1–2, pp. 48–60, Sep. 1986.
[10] A. Ramesh, D. C. Jiles, and J. M. Roderick, "A model of anisotropic anhysteretic magnetization," *IEEE Trans. Magn.*, vol. 32, no. 5, pp. 4234–4236, Sep. 1996.
[11] R. Szewczyk, "Validation of the anhysteretic magnetization model for soft magnetic materials with perpendicular anisotropy," *Materials*, vol. 7, no. 7, pp. 5109–5116, Jul. 2014.
[12] I. D. Mayergoyz, *Mathematical Models of Hysteresis and Their Applications*. New York, NY, USA: Academic, 2003.
[13] S. Bobbio, G. Miano, C. Serpico, and C. Visone, "Models of magnetic hysteresis based on play and stop hysterons," *IEEE Trans. Magn.*, vol. 33, no. 6, pp. 4417–4426, Nov. 1997.
[14] S. Steentjes, K. Hameyer, D. Dolinar, and M. Petrun, "Iron-loss and magnetic hysteresis under arbitrary waveforms in, no. electrical steel: A comparative study of hysteresis models," *IEEE Trans. Ind. Electron.*, vol. 64, no. 3, pp. 2511–2521, Mar. 2016.
[15] S. E. Zirka, Y. I. Moroz, R. G. Harrison, and N. Chiesa, "Inverse hysteresis models for transient simulation," *IEEE Trans. Power Del.*, vol. 29, no. 2, pp. 552–559, Apr. 2013.
[16] S. E. Zirka, Y. I. Moroz, P. Marketos, and A. J. Moses, "Congruency-based hysteresis models for transient simulation," *IEEE Trans. Magn.*, vol. 40, no. 2, pp. 390–399, Mar. 2004.
[17] L. Dupre, R. Van Keer, J. Melkebeek, Y. Moroz, and S. Zirka, "Hysteresis models for transient simulation," in *Scientific Computing in Electrical Engineering*. Berlin, Germany: Springer, 2001, pp. 105–112.
[18] D. Jiles, *Introduction to Magnetism and Magnetic Materials*. Boca Raton, FL, USA: CRC Press, 2015.
[19] *Magnetic Materials—Methods of Measurement of the Magnetic Properties of Electrical Sheet and Strip by Means of a Single Sheet Tester*, Standard BS EN 10280:2001 +A1:2007, 2007.
[20] *The Expression of Uncertainty and Confidence in Measurement*, 4th ed. U.K.: United Kingdom Accreditation Service, Oct. 2019.
[21] H. Hamzehbahmani, P. Anderson, and K. Jenkins, "Interlaminar insulation faults detection and quality assessment of magnetic cores using flux injection probe," *IEEE Trans. Power Del.*, vol. 30, no. 5, pp. 2205–2214, Oct. 2015.